



# A coupled volume-of-fluid and level set (VOSET) method for computing incompressible two-phase flows

D.L. Sun, W.Q. Tao\*

State Key Laboratory of Multiphase Flow in Power Engineering, School of Energy & Power Engineering, Xi'an Jiaotong University, Xi'an, Shaanxi 710049, PR China

## ARTICLE INFO

### Article history:

Received 24 February 2009  
Received in revised form 28 August 2009  
Accepted 23 September 2009  
Available online 10 November 2009

### Keywords:

VOF method  
LS method  
VOSET method  
Volume fraction function  
Level set function

## ABSTRACT

A coupled volume-of-fluid and level set (VOSET) method, which combines the advantages and overcomes the disadvantages of VOF and LS methods, is presented for computing incompressible two-phase flows. In this method VOF method is used to capture interfaces, which can conserve the mass and overcome the disadvantage of nonconservation of mass in LS method. An iterative geometric operation proposed by author is used to calculate the level set function  $\phi$  near interfaces, which can be applied to compute the accurate curvature  $\kappa$  and smooth the discontinuous physical quantities near interfaces. By using the level set function  $\phi$  the disadvantages of VOF method, inaccuracy of curvature and bad smoothness of discontinuous physical quantities near interfaces, can be overcome. Finally the computing results made with VOSET method are compared with those made with VOF and LS methods.

© 2009 Published by Elsevier Ltd.

## 1. Introduction

Flows with a spatial variation of fluid properties, such as gas-liquid interfaces due to density and viscosity differences, can be found in many natural and industrial processes such as chemical reactor, power plant, copper refining and internal combustion engine. The generation of vorticity by the discontinuous fluid properties produces a complex flow structure, which presents a computational challenge.

In the past several decades a number of different methods have been developed to simulate complex two-phase flow problems. The most important methods include the front tracking method [1–4], the marker particle method [5,6], the volume of fluid (VOF) method [7–17] and the level set (LS) method [18–24]. Since the development of VOF method by Hirt and Nichols [7] in 1981, the method has become very popular and is widely used in the free-surface modeling. The LS method was developed in 1988 by Osher and Sethian [18]. It has become popular in many disciplines, such as image processing, computer graphics, computational geometry and computational physics. Thus, among the four major methods mentioned above, the VOF method and LS method are probably the most widely used methods in the literatures. Needless to say, each method has its own advantages and drawbacks. In the present work based on a comprehensive analysis to VOF and LS methods, a coupled volume-of-fluid and level set method (hereafter VOSET), which combines the

advantages and overcomes the disadvantages of VOF and LS methods, is presented for computing the incompressible two-phase flows. In the following a brief review on the VOF and LS methods and their advantages/disadvantages are presented.

In the VOF method, a volume fraction function  $C$ , whose value lies between 0 and 1, is defined to denote whether a space is occupied by the dispersed phase or continuous phase. When the value of  $C$  is unity, the space is occupied by the dispersed phase; when the value of  $C$  is zero, the space is occupied by the continuous phase; when the value of  $C$  is between 0 and 1, the space contains both the dispersed and continuous phases, where by the definition a free surface exists.

For a given flow field, the standard advection equation governs the evolution of  $C$ :

$$\frac{\partial C}{\partial t} + \vec{u} \cdot \nabla C = 0 \quad (1)$$

If the flow is incompressible, the  $C$  advection equation can be recast in the conservative form:

$$\frac{\partial C}{\partial t} + \nabla \cdot (\vec{u}C) = 0 \quad (2)$$

For the  $C$  advection equation, the standard finite-difference approximations would lead to a smearing of the  $C$  function and the interfaces would lose their definition. Therefore, the volume tracking algorithms are applied to capture the interfaces. Most volume tracking algorithms published to date fall into one of these two interface reconstruction categories: one is the Piecewise Constant Volume

\* Corresponding author. Tel./fax: +86 29 82669106.  
E-mail address: [wqtao@mail.xjtu.edu.cn](mailto:wqtao@mail.xjtu.edu.cn) (W.Q. Tao).

Tracking Methods, which include Hirt and Nichols's donor-acceptor algorithm [7]; the other is the Piecewise Linear Volume Tracking Methods, which include the PLIC (Piecewise Linear Interface Construction) algorithm due to Youngs [8]. In our study the PLIC algorithm is adopted to solve Eq. (2) and reconstruct the interfaces, because this algorithm is more accurate than other algorithms.

Usually, in the VOF method the smoothed volume fraction function  $\tilde{C}$  is used to compute the curvature  $\kappa$ . The smoothed volume fraction function  $\tilde{C}$  can be obtained by

$$\tilde{C}_{ij} = \sum_{m,n} C_{m,n} K(|\vec{r}_{ij} - \vec{r}_{m,m}|, \varepsilon) \delta x \delta y \quad (3)$$

where the smoothening function  $K$  is given by the cubic B-spline proposed by Monaghan [25]:

$$K(r, \varepsilon) = \begin{cases} \frac{40}{7\pi} \left(1 - 6\left(\frac{r}{\varepsilon}\right)^2 + 6\left(\frac{r}{\varepsilon}\right)^3\right) & \text{if } \frac{r}{\varepsilon} < \frac{1}{2} \\ \frac{80}{7\pi} \left(1 - \frac{r}{\varepsilon}\right)^3 & \text{if } \frac{1}{2} \leq \frac{r}{\varepsilon} < 1 \\ 0 & \text{otherwise} \end{cases} \quad (4)$$

where  $\varepsilon$  denotes the width of transition region used for smoothening. In the present paper typically  $\varepsilon = 3\Delta$  is used in the VOF method where  $\Delta$  represents the grid size.

The curvature  $\kappa$  can be obtained by the following equation:

$$\kappa = - \left( \nabla \cdot \frac{\nabla \tilde{C}}{|\nabla \tilde{C}|} \right) \quad (5)$$

The curvature can also be written as

$$\kappa = \frac{1}{|\nabla \tilde{C}|} \left[ \left( \frac{\nabla \tilde{C}}{|\nabla \tilde{C}|} \cdot \nabla \right) |\nabla \tilde{C}| - \left( \nabla \cdot \nabla \tilde{C} \right) \right] \quad (6)$$

The curvature value numerically calculated by Eq. (5) is quite inaccurate, because the principal contributions to Eq. (5) come from the edges of the transition region rather than center. However, numerical approximations to Eq. (6), for which the principal contributions come from the center of the transition region, give better results in practice [26]. So Eq. (6) is adopted to calculate the curvature in the VOF method.

The discontinuous physical quantities (density and viscosity) near interfaces can be smoothed by

$$\rho(C) = \rho_d C + \rho_c (1 - C) \quad (7)$$

$$\mu(C) = \mu_d C + \mu_c (1 - C) \quad (8)$$

where the subscripts  $d$  and  $c$  denote, respectively, the dispersed and continuous phases.

An advantage of VOF method is the fact that accurate algorithms can be used to advect the volume fraction function so that the mass is conserved while still maintaining a sharp representation of the interfaces [27]. However, because the volume fraction function  $C$  is a step function, it is difficult to obtain the accurate curvature and smooth the discontinuous physical quantities near the interfaces. Even though the smoothed volume fraction function  $\tilde{C}$  is used to compute the curvature, the accuracy of the curvature is still not good. This is the disadvantage of VOF method [27].

In the LS method, a smooth function  $\phi$ , called level set function, is used to represent the interfaces. Generally, a signed distance function, on which an extra condition of  $|\nabla \phi| = 1$  is imposed, is defined as the level set function. The signed distance function can be expressed as

$$\phi(\vec{r}, t) = \begin{cases} -d(\vec{r}, \Gamma(t)) < 0 & \text{if } \vec{r} \in \text{the dispersed phase,} \\ = 0, & \text{if } \vec{r} \in \text{the interface,} \\ d(\vec{r}, \Gamma(t)) > 0 & \text{if } \vec{r} \in \text{the continuous phase.} \end{cases} \quad (9)$$

where  $\Gamma$  denotes the interfaces,  $d$  is the distance function which is the shortest distance from some point to the interfaces. In the LS method, the location is indicated by  $\phi$ :  $\phi < 0$  in the dispersed-phase region,  $\phi > 0$  in the continuous-phase region, and  $\phi = 0$  on the interfaces.

Since the interfaces move with fluid flow, the evolution of  $\phi$  is given by

$$\frac{\partial \phi}{\partial t} + \vec{u} \cdot \nabla \phi = 0 \quad (10)$$

In order to keep the solution accurate, the level set function  $\phi$  needs to be reinitialized after every time step. This is achieved by solving the following transient problem to the steady state:

$$\begin{cases} \phi_\tau = S(\phi_0)(1 - |\nabla \cdot \phi|) \\ \phi(\vec{r}, 0) = \phi_0(\vec{r}) \end{cases} \quad (11)$$

where  $\phi_\tau$  is the time derivative and  $S$  is the sign function. Eq. (11) has the property that  $\phi$  remains unchanged at the interfaces, therefore,  $\phi_0$  and  $\phi$  at the zero level set are the same. In Eq. (11) the level set function  $\phi$  will converge to  $|\nabla \phi|=1$  with the evolution of time. Although this approach improves conservation of mass considerably, it fails to achieve mass conservation exactly.

From the level set function the curvature  $\kappa$  can be obtained by the following equation:

$$\kappa = \left( \nabla \cdot \frac{\nabla \phi}{|\nabla \phi|} \right) \quad (12)$$

For smoothing the discontinuous physical quantities near interfaces, the smoothed Heaviside function is used which is given by

$$H_\varepsilon(\phi) = \begin{cases} 0 & \text{if } \phi < -\varepsilon \\ \frac{1}{2} \left[ 1 + \frac{\phi}{\varepsilon} - \frac{1}{\pi} \sin(\pi \phi / \varepsilon) \right] & \text{if } |\phi| \leq \varepsilon \\ 1 & \text{if } \phi > \varepsilon \end{cases} \quad (13)$$

Typically  $\varepsilon = 1.5\Delta$  is used where  $\Delta$  represents the grid size. Then the smoothed density and viscosity can be calculated by

$$\rho_\varepsilon(\phi) = \rho_d(1 - H_\varepsilon(\phi)) + \rho_c H_\varepsilon(\phi) \quad (14)$$

$$\mu_\varepsilon(\phi) = \mu_d(1 - H_\varepsilon(\phi)) + \mu_c H_\varepsilon(\phi) \quad (15)$$

The advantages of LS method are the fact that the curvature can be computed accurately and the smoothness of discontinuous physical quantities near interfaces is very good by using the level set function  $\phi$  – a smooth function.

However, the LS method produces more numerical error than VOF method, especially when the interfaces experience severe stretching or tearing. A common symptom of such a disadvantage is the loss/gain of mass. To alleviate the problem of mass being not conserved, Sussman et al. [20] have developed a constraint that significantly improves the accuracy of solving Eq. (11). Nourgaliev et al. [28] have showed that reducing the spatial discretization errors in Eq. (10) can improve mass conservation. The fast marching method [29] is another technique for calculating distance functions, which can improve mass conservation property. However, it must be noted that none of the above techniques can exactly conserve mass. This is the disadvantage of LS method [27].

On the basis of the above analysis to VOF and LS methods, it can be found that they have the complementary advantages and disadvantages, so it is an inevitable trend to develop a method combining the VOF and LS methods.

In 2000 a CLSVOF method, which combines the VOF and LS methods, was put forward by Sussman [27]. Although this method extracts the advantages of VOF and LS methods, it is more complicated than VOF or LS method. Because in this method both the  $C$  and  $\phi$  advection equations need to be solved, and the level set function needs to be coupled to the volume fraction function by assigning the level set function to be the exact signed normal dis-

tance to the reconstructed interfaces. Subsequently, improved CLSVOF [30], MCLS [31] and ACLSVOF [32] methods were put forward. Just as the original CLSVOF, all of these methods need to solve both the  $C$  and  $\phi$  advection equations.

The present coupled volume-of-fluid and level set (VOSET) method is simpler than CLSVOF method and the others mentioned above. This is because in the present method only the  $C$  advection equation needs to be solved and the level set function is calculated by a simple iterative geometric operation. In the following the VOSET method will first be introduced in detail. Then four examples of the incompressible two-phase flow will be illustrated to compare the VOF, LS and VOSET methods. For the simplicity of presentation, all the derivations and computations are conducted on the uniform grids in two-dimensional Cartesian coordinates.

**2. Iterative geometric operation to calculate the level set function**

Before calculating the level set function by iterative geometric operation, the interface shapes and locations should be firstly confirmed by reconstructing the interfaces. In PLIC algorithm the interface reconstruction is based on the idea that a normal vector together with the volume fraction  $C$  determines a unique linear interface cutting the cell. The normal vector to an interface is estimated by a finite-difference formula of the following equation:

$$\vec{n} = \nabla C / |\nabla C| \tag{16}$$

There are 16 possible cases for the interface shape in the PLIC algorithm. For  $n_x > 0$  and  $n_y > 0$  there exist 4 cases as shown in Fig. 1.

After the interface shape is reconstructed based on the PLIC algorithm, the level set function  $\phi$ , i.e. the signed distance function, can be calculated by an iterative geometric operation. The detailed procedure of the operation is presented as follows:

*Step 1:* Set the initial value for the signed distance function  $\phi$  in the whole computational domain.

$$\phi_{ij}^0 = \begin{cases} -M & \text{if } C_{ij} \geq 0.5 \\ M & \text{if } C_{ij} < 0.5 \end{cases} \tag{17}$$

where  $M$  is the max geometrical size of physical model as shown in Fig. 2. This can guarantee that the accurate signed distance function near the interfaces is included in the initial value of  $\phi$ , i.e.  $-M < \phi < M$ .

*Step 2:* Flag the cells near the interfaces. We flag the cells in the region of  $3-\Delta$  width on each side of the interfaces where  $\Delta$  represents the grid size, as shown in Fig. 3. Such flagged region is wide enough to compute the curvature  $\kappa$  and smooth the discontinuous physical quantities near the interfaces. This flagging step can avoid calculating the signed distance function in the whole computational domain and thus can save computational time.

*Step 3:* Calculate the signed distance function  $\phi$  in the flagged region near the interfaces. Before calculating the signed distance function  $\phi$ , we should first compute the shortest distance  $d$  to the interfaces for each grid point within the flagged region. The shortest distance from grid point  $(i, j)$  to the interfaces can be ob-

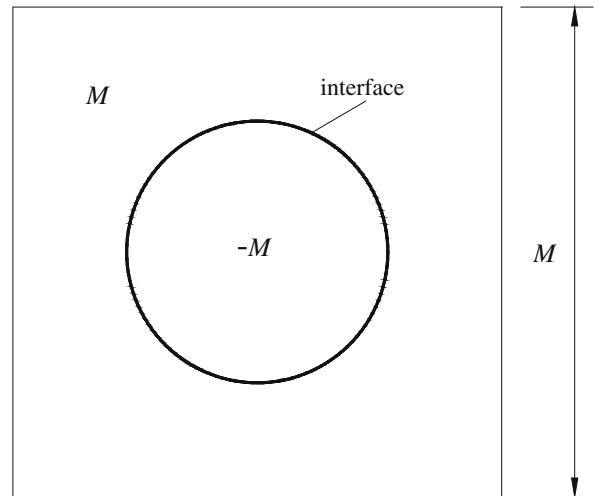


Fig. 2. Initial value  $\phi_0$  of the signed distance function.

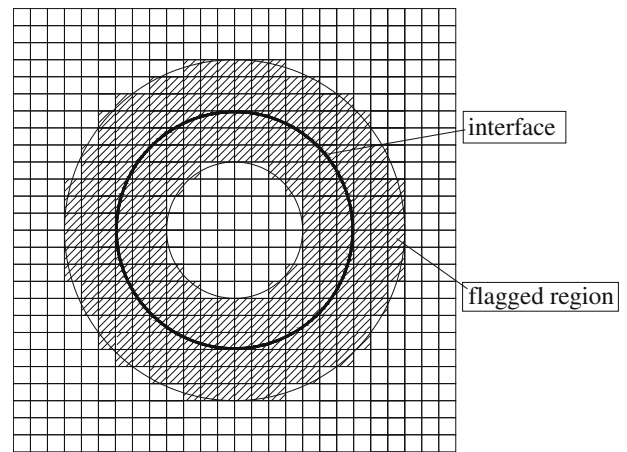


Fig. 3. The flagged region near interfaces.

tained by comparing all of the minimum distances from grid point  $(i, j)$  to any interface in cells within a  $7 \times 7$  stencil around the cell  $(i, j)$ . The reason of selecting  $7 \times 7$  stencil to compute the shortest distance is that the signed distance function is calculated only in the region of  $3-\Delta$  width on each side of the interfaces.

Fig. 4 shows the method of calculating the minimum distance to an interface in a cell. In the figure, the thick line segment BC denotes the interface. When  $\theta_1 > 90^\circ$ , AB is the minimum distance; when  $\theta_2 < 90^\circ$ , AC is the minimum distance; when  $\theta_1 < 90^\circ$  and  $\theta_2 < 90^\circ$ , the line AD vertical to the interface is the minimum distance.

The shortest distance from grid point  $(i, j)$  to interfaces can be obtained by comparing all of the minimum distances to any inter-

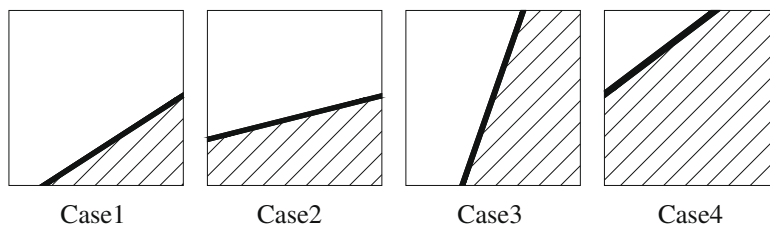


Fig. 1. The interface shape in computational cell for  $n_x > 0$  and  $n_y < 0$ .

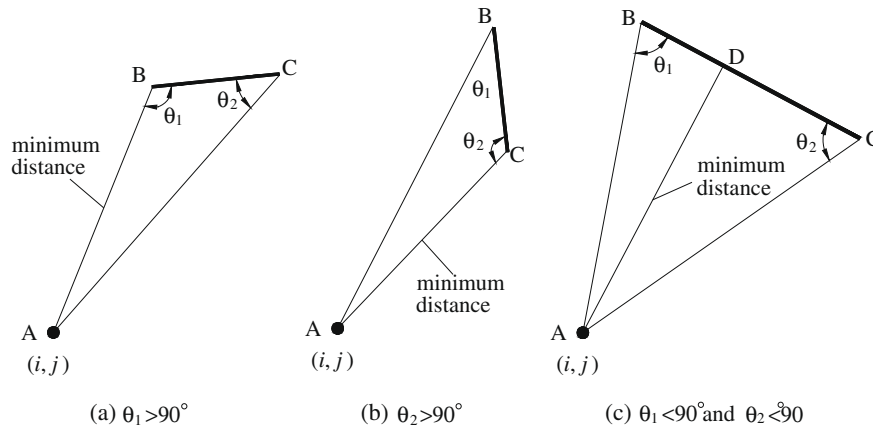


Fig. 4. The minimum distance to an interface in a cell.

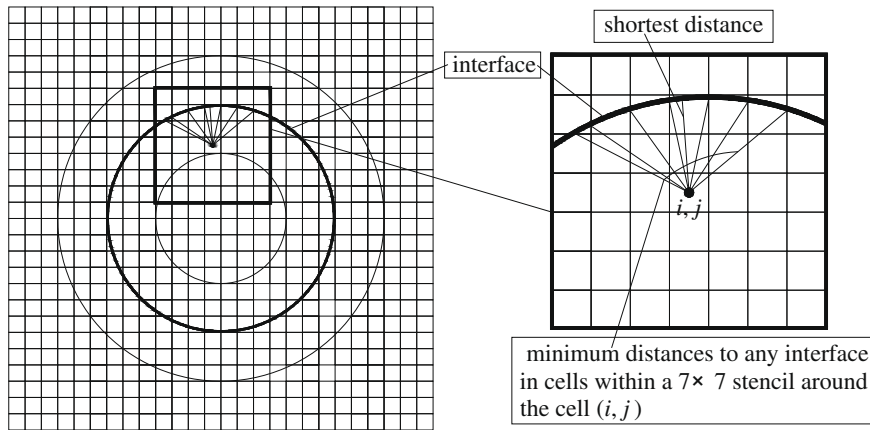


Fig. 5. The shortest distance determined by comparing all of the minimum distances.

face in cells within the  $7 \times 7$  stencil around the cell  $(i, j)$ , as shown in Fig. 5. The signed distance function can be obtained by

$$\phi_{ij} = \begin{cases} -d & \text{if } C_{ij} > 0.5 \\ 0 & \text{if } C_{ij} = 0.5 \\ d & \text{if } C_{ij} < 0.5 \end{cases} \quad (18)$$

Then the normal vector to the interface is calculated again with the signed distance function by the following equations:

$$\vec{n} = \nabla\phi / |\nabla\phi| \quad (19)$$

Based on the more accurate normal vector determined by Eq. (19), the interface is reconstructed again. Then return to Step 1. Repeat the geometric operation until the iteration times is equal to the pre-specified times  $N$ . By the iteration, we can acquire more accurate signed distance function. Usually, the iteration times  $N$  is set as 1 for coarse mesh and 3 for fine mesh.

Fig. 6 shows the signed distance function near the interfaces with different shapes, which is calculated by the iterative geometrical operation. In Fig. 6 the thick lines denote the interfaces and the thin lines represent the contour lines of the signed distance function. From Fig. 6 we can find that accurate signed distance functions can be calculated by the proposed iterative geometrical operation.

It is worth noting that the above-mentioned method for determining the level-set function is the major novelty of the present paper. Because the simplicity of the proposed method the present

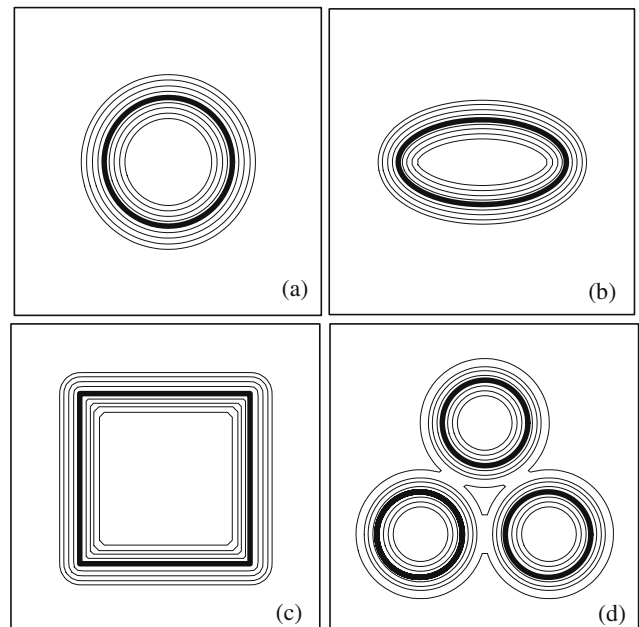


Fig. 6. The signed distance function near the interfaces with different shapes calculated by the iterative geometrical operation.

coupled VOF and LS method (VOSET) is much simpler than all existing coupled variants, while still keeps the advantages of the two original ones.

### 3. Advection of volume fraction function

The discretization form of Eq. (2) is expressed as

$$C^{n+1} = C^n - \delta t \nabla \cdot (C^n \bar{u}^n) \quad (20)$$

For decreasing the errors induced by the mass residual, Eq. (20) can be modified as

$$C^{n+1} = C^n - \delta t \nabla \cdot (C^n \bar{u}^n) + \delta t C^n \nabla \cdot (\bar{u}^n) \quad (21)$$

In this paper the PLIC algorithm is applied to solve Eq. (21). The interface reconstruction is the same as that mentioned above. The signed distance function, acquired by the iterative geometric operation, is used to calculate the normal vector to the interface. After the interface shape is reconstructed, the operator splitting is applied for the time integration.

### 4. Applications of the level set function

After the level set function, i.e. the signed distance function, is calculated by the iterative geometrical operation, we can compute the curvature by Eq. (12) and smooth the density and viscosity by Eqs. (14) and (15). In addition, the surface pressure caused by the existence of phase interface can also be determined from the level set function.

Based on the CSF (Continuum Surface Force) model [26], the surface pressure is expressed as follows [19,20]:

$$F_{sv} = -\sigma \kappa(\phi) \delta_\varepsilon(\phi) \nabla \phi \quad (22)$$

The smoothed delta function is

$$\delta_\varepsilon(\phi) = \frac{dH_\varepsilon(\phi)}{d\phi} \quad (23)$$

where  $\varepsilon = 1.5\Delta$ .

### 5. Governing equations and their discretizations

For incompressible two-phase flows the Navier–Stokes equations for the dispersed-phase and continuous-phase fluids can be combined into a set of equations in an entire domain. The governing equations for transient, incompressible, Newtonian, two-phase flows are given by the following expressions:

$$\nabla \cdot \bar{u} = 0 \quad (24)$$

$$\frac{\partial \bar{u}}{\partial t} + \bar{u} \nabla \cdot (\bar{u}) = \frac{1}{\rho_\varepsilon(\phi)} \left\{ -\nabla p + \nabla \cdot \mu_\varepsilon(\phi) [(\nabla \bar{u}) + (\nabla \bar{u})^T] + \rho_\varepsilon(\phi) \bar{g} - \sigma \kappa \nabla H_\varepsilon \right\} \quad (25)$$

The governing equations are discretized based on the Finite Volume Method (FVM) [33,34]. We use the high order ENO upwind differencing [35] for the convection term and the central differencing for the viscous and curvature terms. The equations are advanced in time by using the second order TVD Runge–Kutta method.

### 6. Solution procedure of VOSET method

In the solution procedure of VOSET method the second order projection method is adopted, which is based on the second order TVD Runge–Kutta method. The solution procedure of the VOSET method is presented as follows.

*Step 1:* Calculate the temporary  $C_{Temp}^{n+1,(0)}$ ,  $\bar{u}_{Temp}^{n+1,(0)}$  and  $p_{Temp}^{n+1,(0)}$  on the time  $(n+1,(0))$  level based on the  $C^n$ ,  $\bar{u}^n$  and  $p^n$ .

- (1) The signed distance function  $\phi^n$  near the interfaces is calculated by the iterative geometric operation and is used to calculate the curvature (Eq. (12)) and smooth the discontinuous physical quantities near the interfaces (Eqs. (14), (15)).
- (2) The PLIC algorithm is applied to calculate the  $C_{Temp}^{n+1,(0)}$  on the time  $(n+1,(0))$  level (Eq. (21)).
- (3) An intermediate velocity is evaluated by

$$\bar{u}^* = \bar{u}^n - \delta t \bar{u}^n \nabla \cdot (\bar{u}^n) + \frac{\delta t}{\rho_\varepsilon(\phi^n)} \left\{ -\nabla p^n + \nabla \cdot \mu_\varepsilon(\phi^n) [(\nabla \bar{u}^n) + (\nabla \bar{u}^n)^T] + \rho_\varepsilon(\phi^n) \bar{g} - \sigma \kappa(\phi^n) \delta_\varepsilon(\phi^n) \nabla \phi^n \right\} \quad (26)$$

- (4) Following pressure-correction equation is solved

$$\nabla \cdot \left( \frac{1}{\rho_\varepsilon(\phi^n)} \nabla p' \right) = \frac{1}{\delta t} \nabla \cdot \bar{u}^* \quad (27)$$

The pressure-correction equation is solved by using a very robust and efficient Krylov subspace method: Bi-CGSTAB algorithm proposed by Van Der Vorst [36,37].

- (5) The temporary velocity and pressure on the time  $(n+1,(0))$  level can be obtained from

$$\bar{u}_{Temp}^{n+1,(0)} = \bar{u}^* - \frac{\delta t}{\rho_\varepsilon(\phi^n)} \nabla p' \quad (28)$$

$$p_{Temp}^{n+1,(0)} = p^n + p' \quad (29)$$

*Step 2:* Calculate the temporary  $C_{Temp}^{n+1,(1)}$ ,  $\bar{u}_{Temp}^{n+1,(1)}$  and  $p_{Temp}^{n+1,(1)}$  on the time  $(n+1,(1))$  level based on the temporary  $C_{Temp}^{n+1,(0)}$ ,  $\bar{u}_{Temp}^{n+1,(0)}$  and  $p_{Temp}^{n+1,(0)}$ . The solution process is the same as that mentioned in *Step 1*.

*Step 3:* Calculate the  $C^{n+1}$ ,  $\bar{u}^{n+1}$  and  $p^{n+1}$  on the time  $(n+1)$  level by the following equations:

$$C^{n+1} = (C_{Temp}^{n+1,(0)} + C_{Temp}^{n+1,(1)})/2 \quad (30)$$

$$\bar{u}^{n+1} = (\bar{u}_{Temp}^{n+1,(0)} + \bar{u}_{Temp}^{n+1,(1)})/2 \quad (31)$$

$$p^{n+1} = (p_{Temp}^{n+1,(0)} + p_{Temp}^{n+1,(1)})/2 \quad (32)$$

After the  $C^{n+1}$ ,  $\bar{u}^{n+1}$  and  $p^{n+1}$  are acquired, return to *Step 1* and begin the solution on the next time level.

## 7. Results of numerical examples and analysis

In this section, we will compare VOSET method with VOF and LS methods via several examples. In LS method the method for decreasing loss/gain of mass proposed by Sussman [20] has been used. In the following the results of four incompressible, immiscible and non-phase-changed two-phase flow problems with large density and viscosity ratios are presented to compare VOSET method with VOF and LS methods in two-dimensional Cartesian coordinates.

### 7.1. Dam break problem

Firstly, the dam break problem is adopted to validate the VOF, LS and VOSET methods by comparing the numerical results with the experimental data [38].

Fig. 7 shows the physical model of dam break problem. The width of initial liquid column is 0.146 m and the height is 0.292 m. The li-

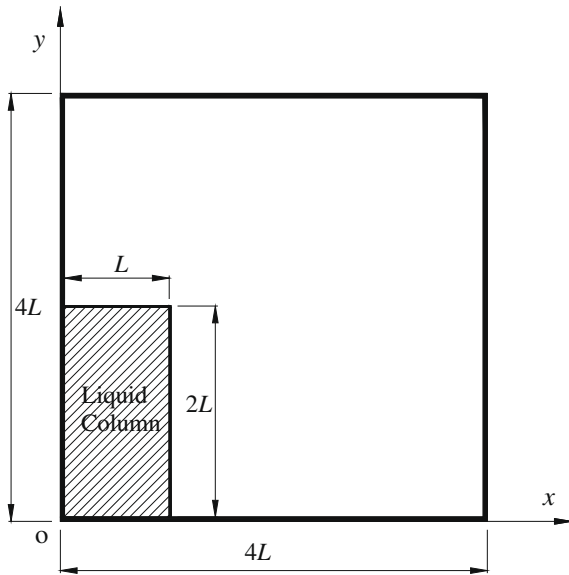


Fig. 7. Physical model of dam break problem.

liquid density  $\rho_l = 1.0 \times 10^3 \text{ kg/m}^3$ , viscosity  $\mu_l = 0.5 \text{ Pa s}$ , background gas density  $\rho_g = 1.0 \text{ kg/m}^3$ , viscosity  $\mu_g = 0.5 \times 10^{-3} \text{ Pa s}$ , gravity  $g = 9.8 \text{ m/s}^2$  and surface tension coefficient  $\sigma = 0.0755 \text{ N/m}$ .

Fig. 8 shows the history of water front marching along the ground surface. As shown in this figure, the numerical results calculated by VOF, LS and VOSET methods agree very well with the experimental data from Martin [38]. By this comparison, it can be proved that the self-developed codes of VOF, LS, and VOSET methods are correct. In the dam break problem, the numerical results of VOF, LS and VOSET methods are almost the same as each other, so it is difficult to compare them. Thereinafter, we will compare these three methods-VOF, LS and VOSET by other three two-phase flow problems.

7.2. Equilibrium circle bubble problem

A gas bubble with radius  $R = 0.5 \text{ m}$ , density  $\rho_g = 1 \text{ kg/m}^3$ , viscosity  $\mu_g = 1.0 \times 10^{-5} \text{ Pa s}$ , background liquid density  $\rho_l = 1000 \text{ kg/m}^3$ , background liquid viscosity  $\mu_l = 1.0 \times 10^{-2} \text{ Pa s}$ , gravity  $g = 0$ , and surface tension coefficient  $\sigma = 0.01 \text{ N/m}$  is located at the center of a box ( $1 \times 1 \text{ m}$ ). In the absence of gravitational force, the circle bubble will be static and keep its circle shape. Here the equilibrium

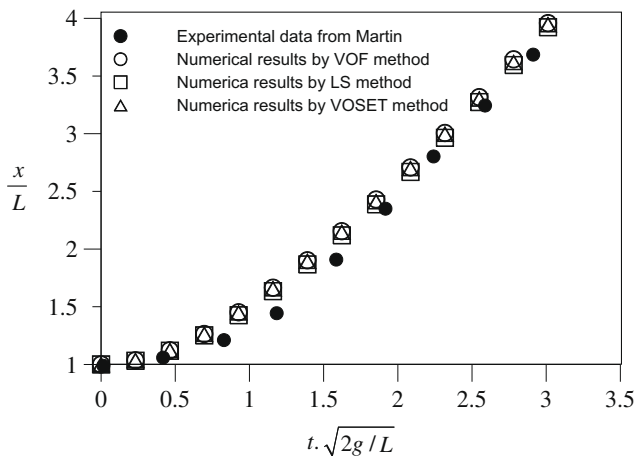


Fig. 8. History of water front marching along the ground surface.

circle bubble problem is adopted to analyze the accuracy of curvature and the smoothness of discontinuous physical quantities near interfaces in VOF, LS, and VOSET methods.

For two-phase flow problems, it is of critical importance to model surface tension accurately, especially to the situation that surface tension is the dominant force affecting the dynamics of fluid flows. The accuracy of surface tension is determined by the accuracy of curvature. In addition the inaccuracy in determining the curvature is one of the important reasons leading to parasitic currents. In VOF method, the smoothed volume fraction function is used to calculate the curvature by Eq. (6). The  $L_2$  error norms for the curvature obtained from the VOF method are present in Table 1. Here the  $L_2$  error norm is defined as

$$L_2 = \sqrt{\frac{\sum_{i=1}^M (\kappa \times R - \kappa_{exact} \times R)^2}{M}} \tag{33}$$

It can be seen that  $L_2$  grows linearly when increasing the mesh resolution in VOF method. The curvatures calculated from the LS method are significantly better than VOF method. In VOSET method, for the coarse mesh  $L_2$  almost keeps unchanged with the increase of iteration times  $N$ ; for the fine mesh  $L_2$  decreases with the increase of  $N$ , i.e. the curvature becomes more accurate with the increase of  $N$ . Usually, the iteration times  $N$  is set as 1 for coarse mesh and 3 for fine mesh. As shown in Table 1, the curvatures obtained from VOSET method are worse than LS method, but much better than VOF method. Thus it can be concluded that VOSET can accurately determine the surface tension and reduce the possible parasitic currents.

For two-phase flow problems, especially with large density and viscosity ratios, the smoothness of density and viscosity is very important for the stability of calculating process and the accuracy of computing results. For the simplicity of presentation, we only compare the smoothed density in the three different methods. In VOF method, the volume fraction function is used to calculate the smoothed density by Eq. (7). In LS and VOSET methods the level set function is applied to calculate the smoothed density by Eq. (14). Fig. 9 shows the contour lines of smoothed density calculated by three different methods. From the figure we can find that the smoothness of density in VOF method is worse than that in LS and VOSET methods. The comparison results of the smoothness of viscosity from the three methods are similar and omitted here.

Fig. 10 shows the bubble pressure calculated by the three different methods. The bubble pressure computed by LS and VOSET methods is smoother than that by VOF method, because the accuracy of curvature and the smoothness of density and viscosity in LS and VOSET methods are much better than those in VOF method.

It is the place to discuss the effects of grid refinement. As shown in Table 1, the  $L_2$  error norm grows linearly when increasing the mesh resolution in VOF method. So the accuracy of VOF method will become worse with the grid refinement. In LS method, the mass loss can reduce gradually with the grid refinement, but it can't exactly conserve mass. With the grid refinement, the VOSET

Table 1

$L_2$  error norms for curvature estimated along a circular interface using the VOF, LS and VOSET methods at different mesh resolutions.

$\Delta x$	VOF	LS	VOSET		
	$L_2$	$L_2$	$N = 1$ $L_2$	$N = 2$ $L_2$	$N = 3$ $L_2$
1/20	0.427	$2.010 \times 10^{-2}$	$4.504 \times 10^{-2}$	$5.362 \times 10^{-2}$	$5.470 \times 10^{-2}$
1/40	0.825	$4.347 \times 10^{-3}$	$5.721 \times 10^{-2}$	$5.712 \times 10^{-2}$	$5.855 \times 10^{-2}$
1/80	0.922	$1.030 \times 10^{-3}$	$8.351 \times 10^{-2}$	$4.678 \times 10^{-2}$	$4.729 \times 10^{-2}$
1/160	1.585	$2.536 \times 10^{-3}$	0.165	$4.033 \times 10^{-2}$	$3.628 \times 10^{-2}$
1/320	3.018	$6.329 \times 10^{-5}$	0.320	$5.311 \times 10^{-2}$	$3.926 \times 10^{-2}$
1/640	6.111	$1.570 \times 10^{-5}$	0.481	$6.898 \times 10^{-2}$	$3.709 \times 10^{-2}$

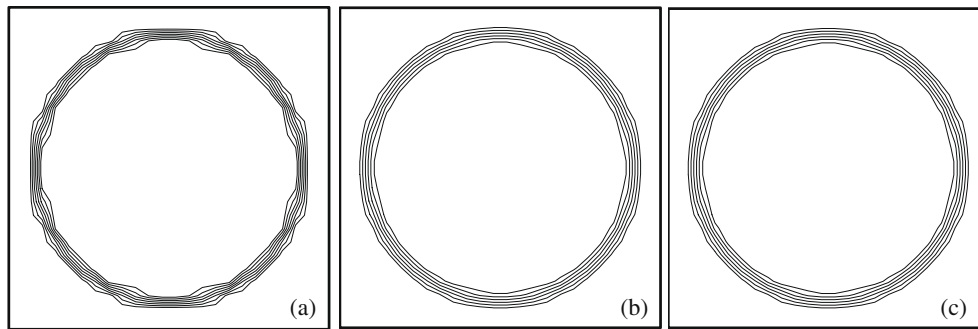


**Fig. 9.** Contour lines of smoothed density calculated by (a) smoothed volume fraction function in VOF method; (b) level set function in LS method; (c) level set function in VOSET method.

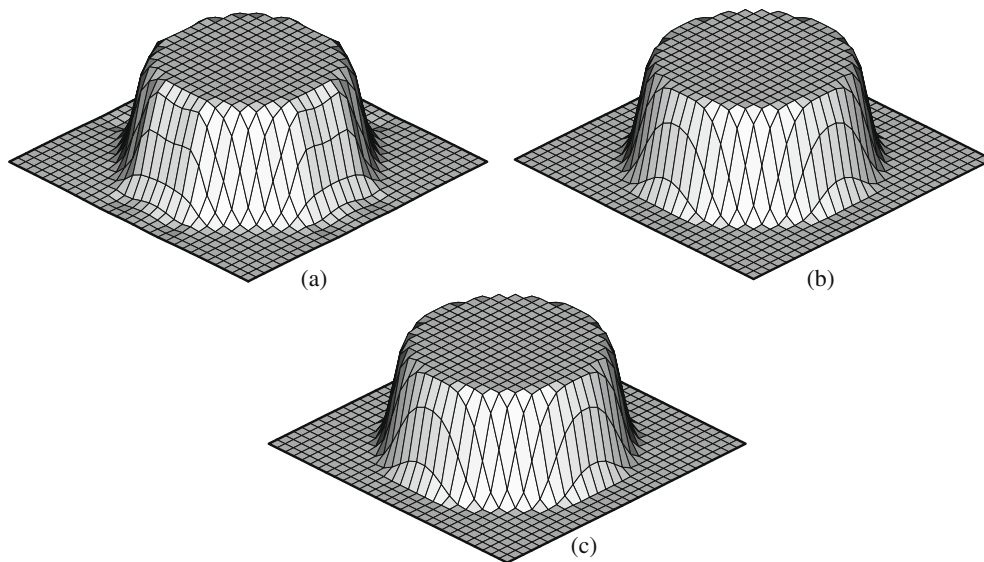


**Fig. 10.** The bubble pressure calculated by (a) VOF method; (b) LS method; (c) VOSET method.

method not only can still conserve mass exactly, but also can keep the accuracy of the curvature. Therefore, it is reasonable to expect that with the grid refinement the advantage of the present method will exhibit more obviously.

### 7.3. Non-equilibrium elliptic bubble problem

An elliptic gas bubble with long axis radius  $R_l = 0.01$  m, short axis radius  $R_s = 0.005$  m, density  $\rho_g = 1$  kg/m<sup>3</sup>, viscosity  $\mu_g = 1.0 \times 10^{-5}$  Pa s, background liquid density  $\rho_l = 1000$  kg/m<sup>3</sup>, background liquid viscosity  $\mu_l = 1.0 \times 10^{-2}$  Pa s, gravity  $g = 0$ , and surface tension coefficient  $\sigma = 0.01$  N/m is located at the center of a box ( $0.05 \times 0.05$  m). Because of the unbalanced surface tension, the elliptic bubble oscillates about its equilibrium shape. In the absence of gravitational force, the surface tension causes the elliptic bubble to become a static circle bubble eventually. Here the evolution time is 5.0 s, which is long enough to let the oscillating bubble keep static.

Fig. 11 shows the oscillating process of an elliptic bubble calculated by the three different methods. In Figs. 11(a1), (b1), (c1) the pressure contour floods are presented, from which we can find that the pressure contour floods calculated by LS and VOSET methods are smoother than that by VOF method. The reason is the same as that mentioned in the equilibrium circle bubble problem.

Because of the unsmoothed pressure in VOF method, the velocity field, especially in the low-viscosity and density phase fluid, is very unstable. As shown in Fig. 11(a2), the velocity field in the

gas-phase fluid computed by VOF method is very disorderly, which differs significantly from that calculated by LS and VOSET methods (Figs. 11(b2) and (c2)). The disorder velocity field leads to the interface shape deviating from that captured by LS/VOSET method as shown in Figs. 11(a2), (b2), (c2). If the topological changes of interfaces are very complicated, the deviation will be much larger. The difference in the interface shape between LS and VOSET methods is very little, implying that at  $t = 0.3$  s the loss/gain of mass in LS method is not serious.

At  $t = 5.0$  s the oscillating elliptic bubble becomes a static circle bubble. The radius of the exact static circle bubble is 0.00707 m. As shown in Figs. 11(a3), (b3), (c3), the gray region denotes the exact static circle bubble and the black line represents the captured interface. From the figure, we can find that the captured interface agrees very well with the interface of the exact static circle bubble in VOF and VOSET methods. However, there exists obvious difference between the captured interface and the exact interface in LS method, which illustrates that the loss/gain of mass is serious at  $t = 5.0$  s.

Fig. 12 shows the variation curve of the ratio of mass with time in this process. Here the ratio is defined as the mass of dispersed-phase fluid on the current time level ( $n$ ) over that on the initial time level (0), i.e.  $\text{Ratio} = M_d^n / M_d^0$ . The exact value of the ratio is equal to 1 in the immiscible, two-phase flows without phase change. As shown in Fig. 12, in LS method the ratio of mass deviates largely from the exact value 1. In VOF and VOSET methods the ratio of mass is almost equal to the exact value 1.

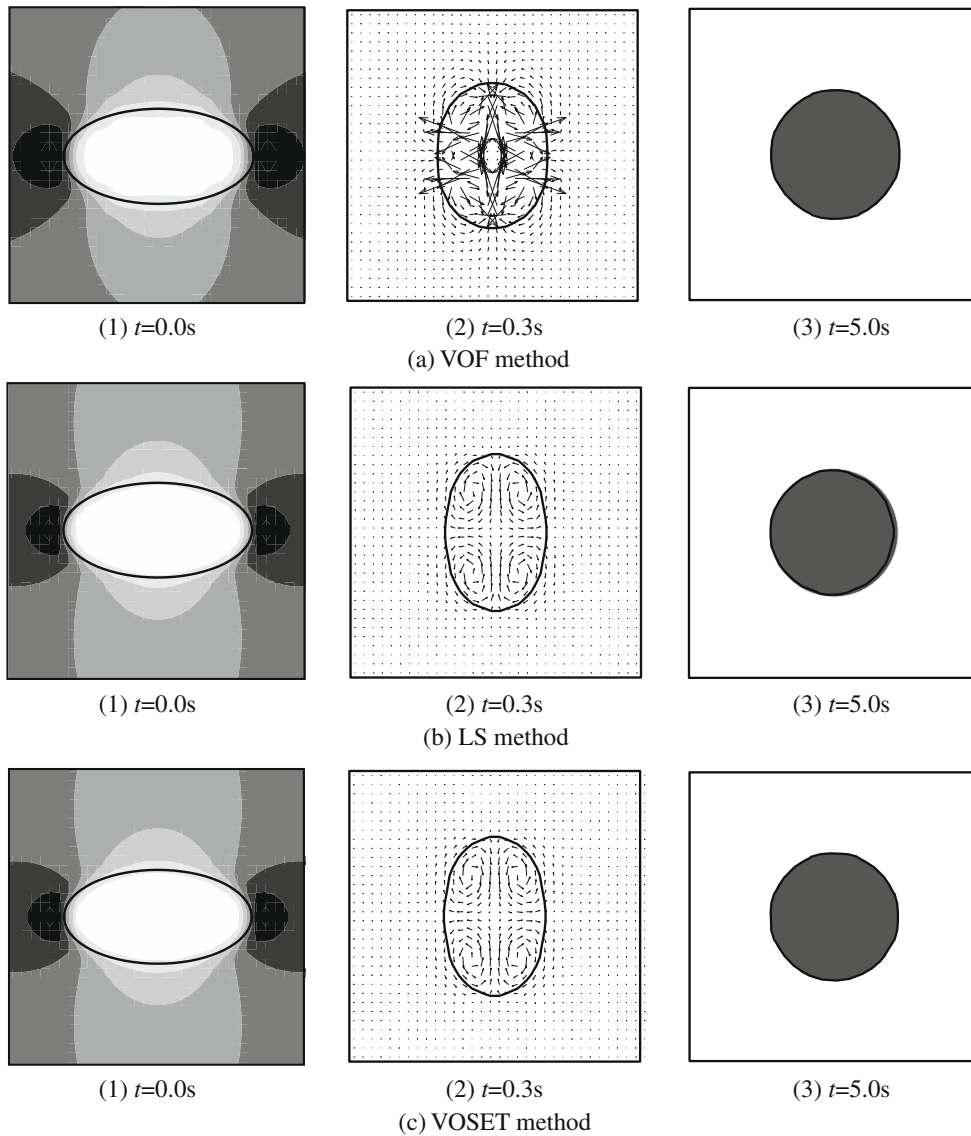


Fig. 11. Oscillating process of an elliptic bubble calculated by (a) VOF method; (b) LS method; (c) VOSET method.

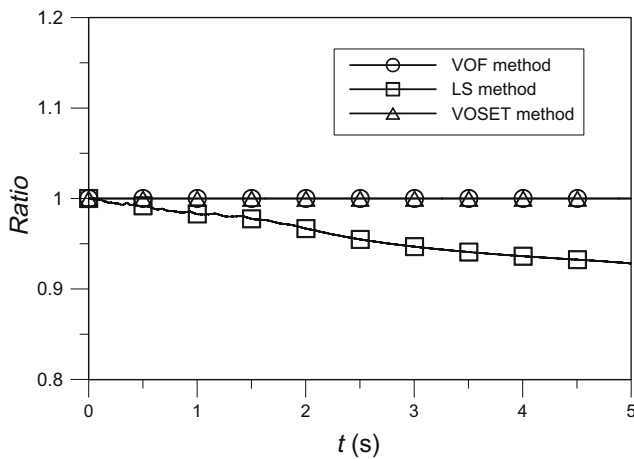


Fig. 12. Variation curve of the ratio of mass with time in the non-equilibrium elliptic bubble problem.

As can be seen from the above comparison, the inaccuracy of curvature and the bad smoothness of discontinuous physical quan-

ties in VOF method make the velocity field in disorder, which leads to the inaccuracy in the interface shape prediction. The non-conservation of mass in LS method also makes the result inaccurate and unreasonable. Thus we can find that the proposed VOSET method can overcome all of these disadvantages, making the results more accurate and reasonable.

#### 7.4. Single gas bubble rising problem

Grace [39] analyzed a lot of experimental data on the properties of single gas bubble rising in an infinite quiescent liquid from different investigators. It was concluded that the relevant physical quantities for single gas bubble rising are determined by four independent dimensionless groups, i.e., Morton number ( $M$ ), Eotvos number ( $Eu$ ), viscosity ratio ( $\kappa$ ), and density ratio ( $\gamma$ ), which are defined by

$$M = g\mu_l^4 / \rho_l \sigma^3 \tag{34}$$

$$Eu = gd_e^2 (\rho_l - \rho_g) / \sigma \tag{35}$$

$$\kappa = \mu_l / \mu_g \tag{36}$$

$$\gamma = \rho_l / \rho_g \tag{37}$$

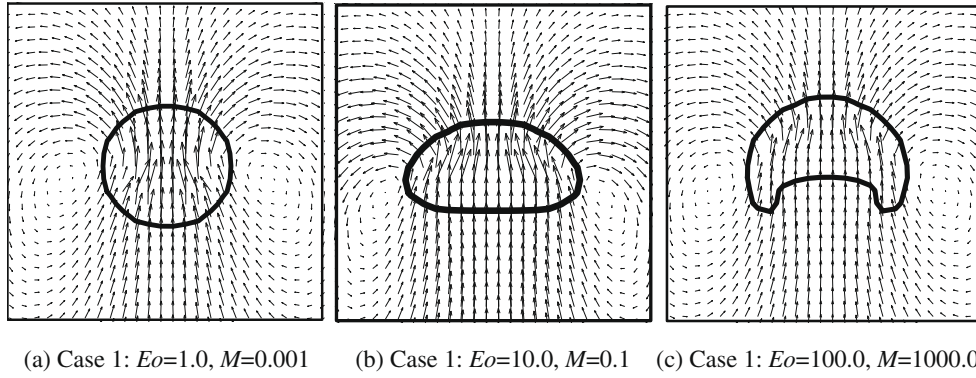


Fig. 13. Bubble terminal shapes computed by VOSET method.

where the subscripts  $g$  and  $l$  denote, respectively, the dispersed gas phase and the continuous liquid phase, and  $d_e$  is the initial bubble diameter.

In this problem a single gas bubble with radius  $R = 0.005$  m is released from the position (0.025 m, 0.02 m) in a quiescent liquid. The domain size is  $0.05 \times 0.15$  m with free slip boundary condition on the walls. The density and viscosity ratios are all set as 1000. Here three different cases are chosen for comparing VOSET method with VOF and LS methods. The first case (case 1) is  $Eo = 1.0$ ,  $M = 0.001$ , the second case (case 2) is  $Eo = 10.0$ ,  $M = 0.1$ , and the third case (case 3) is  $Eo = 100.0$ ,  $M = 1000.0$ . Because of the different surface tension, viscous force and inertial force, the bubble terminal shapes of these three cases are

different as shown in Fig. 13, which is computed by VOSET method.

Fig. 14 shows the variation curve of the ratio of mass with time in the single gas bubble rising problem. As shown in Fig. 14, LS method can't conserve the mass, as indicated by the fact that the ratio deviates largely from the exact value 1 in these three cases. In VOF and VOSET methods the ratio of mass is almost equal to the exact value 1, which shows the mass conservation property of VOF and VOSET methods.

Fig. 15 shows the rising velocity of the single gas bubble with time computed by VOF, LS and VOSET methods. From this picture we can find that the rising velocity computed by VOF method fluctuates largely, especially in case 3. This is because the inaccuracy of

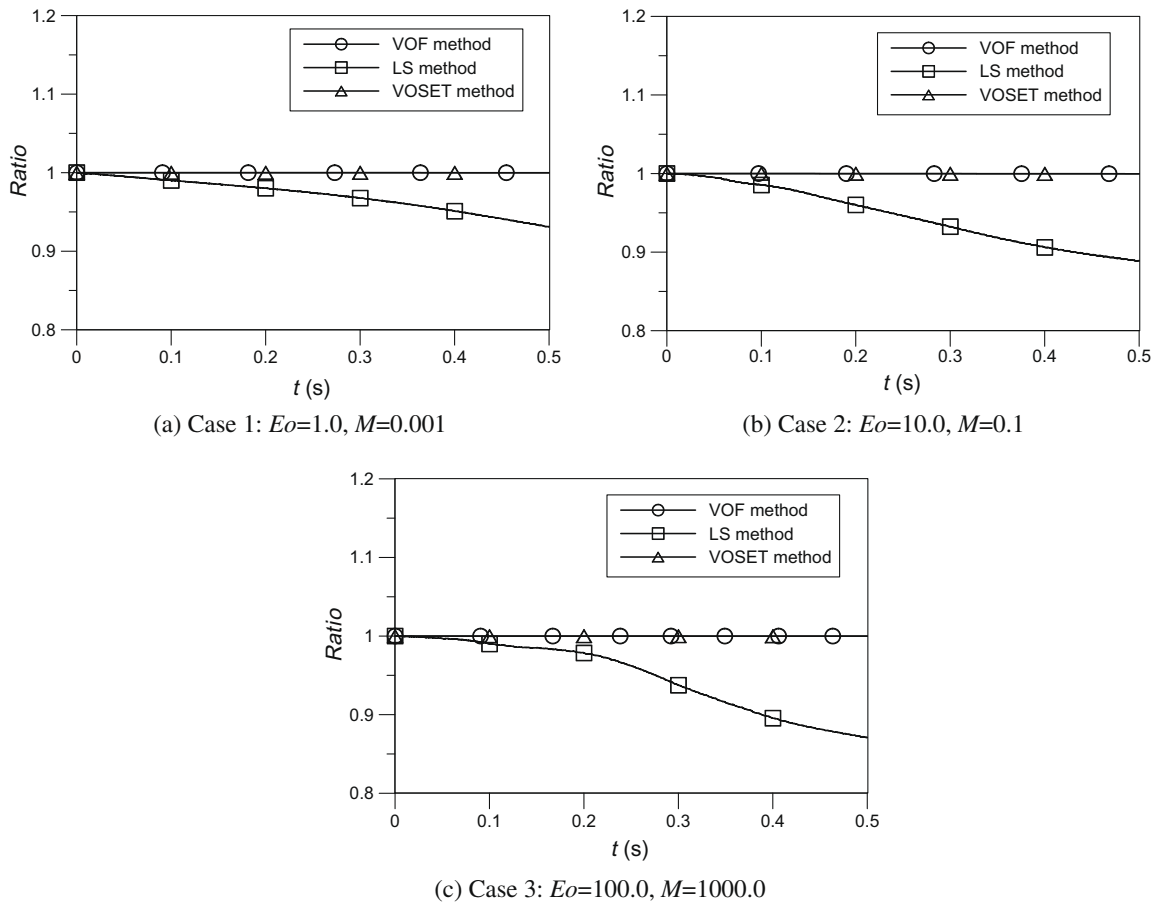


Fig. 14. Variation curve of the ratio of mass with time in the single gas bubble rising problem.

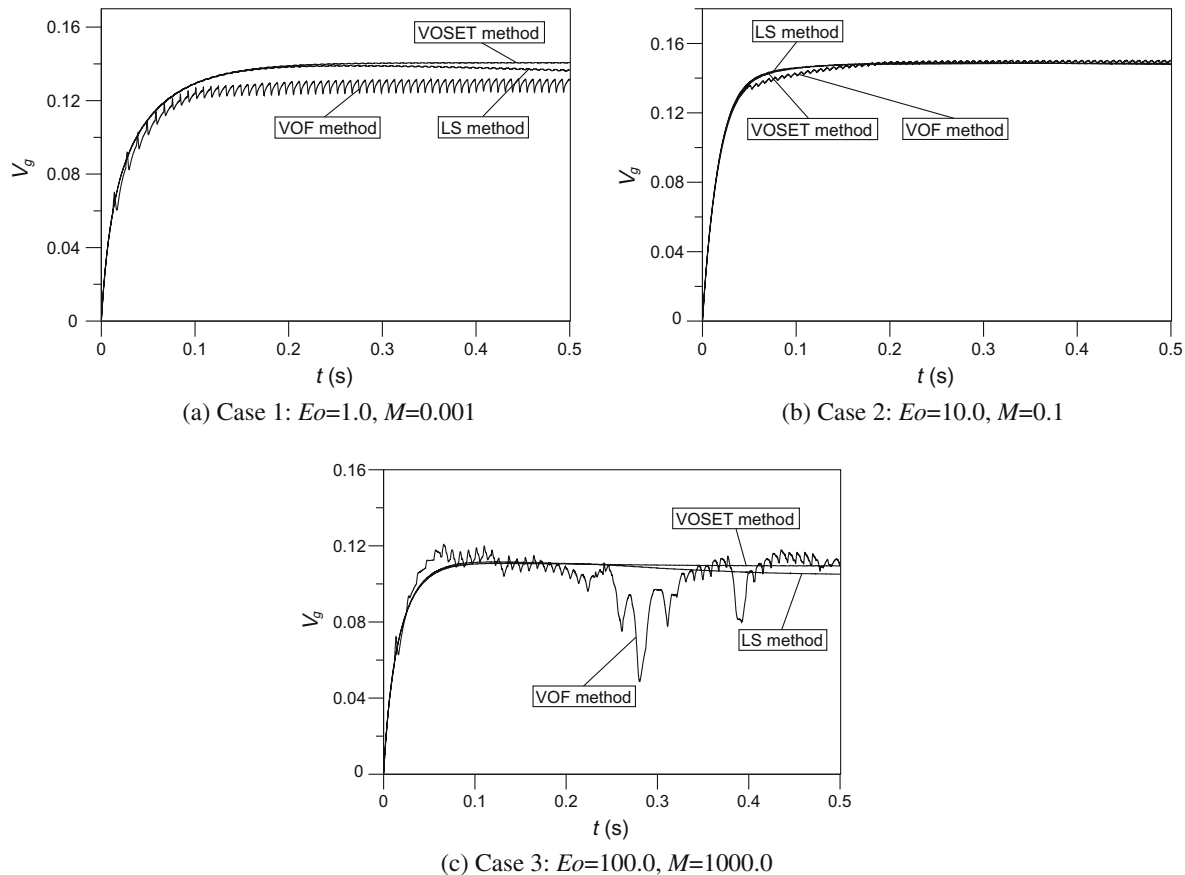


Fig. 15. Rise velocity of single gas bubble with time computed by three different methods.

curvature and the bad smoothness of discontinuous physical quantities make the rising velocity unstable. From this picture we can also find that the rising velocity computed by LS method agrees very well with that computed by VOSET method at the beginning stage. With the advance of time, the difference of the rising velocity becomes larger and larger, which is because the loss/gain of mass is serious at the ending stage in LS method as shown in Fig. 14. The curve of the rising velocity with time computed by VOSET method is very smooth in any case, and only VOSET method can acquire stable terminal velocity as shown in Fig. 15. Therefore, in this regard VOSET method is also more accurate than VOF and LS methods.

Finally it should be noted that all the above examples are two-dimensional to present the major concept of the proposed method. Extending to three dimensional cases, though straightforward in principle, takes much more computational time. It is now underway in the authors' group and will be presented elsewhere.

## 8. Conclusions

A coupled volume-of-fluid and level set (VOSET) method, which combines the advantages and overcomes the disadvantages of VOF and LS methods, has been proposed for computing incompressible two-phase flows without heat transfer. From the comparison of four examples shown above, we can conclude that this method is more accurate than VOF and LS methods. To be specific, the advantages of the proposed VOSET method can be summarized as follows:

- (1) The mass can be conserved exactly. In this method VOF method is used to capture the interfaces, which can exactly conserve the mass and overcome the disadvantage of non-conservation of mass in LS method.

- (2) The signed distance function, obtained by the iterative geometric operation, is used to calculate the curvature and smooth the discontinuity in physical quantities near interfaces. By using the level set function the disadvantage of VOF method, inaccuracy of curvature and bad smoothness of discontinuous physical quantities near interfaces, can be overcome.

In addition, the source code of this method is simple, which can be compiled on the base of VOF and LS methods. Thus it is expected that the proposed VOSET method will be promising in the computations of incompressible two-phase flow and heat transfer problems. Extensions to three-dimensional coordinates, to the case with heat transfer are now underway in the authors' group.

## Acknowledgements

This work was supported by the National Natural Science Foundation of China (50636050, 50876083) and the National Key Project for R&D of China (2007CB206902). Help from Professor M.J. NI in The Graduate School of The Chinese Academy of Science (Beijing) is also greatly acknowledged.

## References

- [1] S.O. Unverdi, G. Tryggvason, A front-tracking method for viscous, incompressible multi-fluid flows, *J. Comput. Phys.* 100 (1992) 25–37.
- [2] A. Esmaeeli, G. Tryggvason, Direct numerical simulation of bubble flows. Part I. Low Reynolds number arrays, *J. Fluid Mech.* 337 (1998) 313–345.
- [3] A. Esmaeeli, G. Tryggvason, Direct numerical simulation of bubble flows. Part II. Moderate Reynolds number arrays, *J. Fluid Mech.* 385 (1998) 325–358.
- [4] G. Tryggvason, B. Bunner, A. Esmaeeli, A front tracking method for the computations of multiphase flow, *J. Comput. Phys.* 169 (2001) 708–759.

- [5] J.E. Welch, F.H. Harlow, J.P. Shannon, B.J. Daly, The MAC method: a computing technique for solving viscous incompressible transient fluid flow problems involving free surfaces, Los Alamos Scientific Laboratory Report LA-3425 (1965).
- [6] W.J. Rider, D.B. Kothe, Stretching and tearing interface tracking methods, Los Alamos Scientific Laboratory, 1995. Available on World Wide Web at: [http://laws.lanl.gov/XHM/personnel/wjr/Web\\_papers/pubs.html](http://laws.lanl.gov/XHM/personnel/wjr/Web_papers/pubs.html).
- [7] C.W. Hirt, B.D. Nichols, Volume of fluid (VOF) method for the dynamics of free boundary, *J. Comput. Phys.* 39 (1981) 201–225.
- [8] D.L. Youngs, Time-dependent Multi-material Flow with Large Fluid Distortion Numerical Method for Fluid Dynamics, Academic, New York, 1982. pp. 273–285.
- [9] N. Ashgriz, J.Y. Poo, FLAIR: flux line-segment model for advection and interface reconstruction, *J. Comput. Phys.* 93 (1991) 449–468.
- [10] W.J. Rider, D.B. Kothe, Reconstructing volume tracking, *J. Comput. Phys.* 141 (1998) 112–152.
- [11] M. Rudman, A volume-tracking method for incompressible multifluid flows with large density variations, *J. Comput. Phys.* 28 (1998) 357–378.
- [12] L. Chen, Y.G. Li, A numerical method for two-phase flows with an interface, *Environm. Model. Software* 13 (1998) 247–255.
- [13] D. Gueyffier, J. Li, A. Nadim, R. Scardovelli, S. Zaleski, Volume-of-fluid interface tracking with smoothed surface stress methods for three-dimensional flows, *J. Comput. Phys.* 152 (1999) 423–456.
- [14] Y. Li, J.P. Zhang, L.S. Fan, Discrete-phase simulation of single bubble rise behavior at elevated pressures in a bubble column, *Chem. Eng. Sci.* 55 (2000) 4597–4609.
- [15] I. Ginzburg, G. Wittum, Two-phase flows on interface refined grids modeled with VOF, staggered finite volume, and spline interpolants, *J. Comput. Phys.* 166 (2001) 302–335.
- [16] D. Lorstad, L. Fuchs, High-order surface tension VOF-model for 3D bubble flows with high density ratio, *J. Comput. Phys.* 200 (2004) 153–176.
- [17] M. van Sint Annaland, N.G. Deen, J.A.M. Kuipers, Numerical simulation of gas bubbles behaviour using a three-dimensional volume of fluid method, *Chem. Eng. Sci.* 60 (2005) 2999–3011.
- [18] S. Osher, J.A. Sethian, Fronts propagating with curvature dependent speed: algorithms based on Hamilton–Jacobi formulations, *J. Comput. Phys.* 79 (1988) 12–49.
- [19] M. Sussman, P. Smereka, S. Osher, A level set approach for computing solutions to incompressible two-phase flow, *J. Comput. Phys.* 114 (1994) 146–159.
- [20] M. Sussman, E. Fatemi, P. Smereka, S. Osher, An improved level set method for incompressible two-phase flows, *Comput. Fluids* 27 (1998) 663–680.
- [21] G. Son, V.K. Dhir, Numerical simulation of film boiling near critical pressures with a level set method, *ASME J. Heat Transfer* 120 (1998) 183–192.
- [22] M. Sussman, A.S. Almgren, J.B. Bell, P. Colella, L.H. Howell, M.L. Welcome, An adaptive level set approach for incompressible two-phase flows, *J. Comput. Phys.* 148 (1999) 81–124.
- [23] G. Son, V.K. Dhir, N. Ramanujapu, Dynamics and heat transfer associated with a single bubble during nucleate boiling on a horizontal surface, *ASME J. Heat Transfer* 121 (1999) 623–631.
- [24] S. Osher, R.P. Fedkiw, Level set methods: an overview and some recent results, *J. Comput. Phys.* 169 (2001) 463–502.
- [25] J.J. Monaghan, Smoothed particle hydrodynamics, *Ann. Rev. Astrophys.* 30 (1992) 543–574.
- [26] J.U. Brackbill, D.B. Kothe, C. Zemach, A continuum method for modeling surface tension, *J. Comput. Phys.* 100 (1992) 335–354.
- [27] M. Sussman, E.G. Puckett, A coupled level set and volume-of-fluid method for computing 3D and axisymmetric incompressible two-phase flows, *J. Comput. Phys.* 162 (2000) 301–337.
- [28] R.R. Nourgaliev, S. Wiri, N.T. Dinh, T.G. Theofanous, On improving mass conservation of level set by reducing spatial discretization errors, *Int. J. Multiphase Flow* 31 (12) (2005) 1329–1336.
- [29] J.A. Sethian, Fast marching methods, *SIAM Rev.* 41 (2) (1999) 199–235.
- [30] G. Son, N. Hur, A coupled level set and volume-of-fluid method for the buoyancy-driven motion of fluid particles, *Num. Heat Transfer B* 42 (2002) 523–542.
- [31] S.P. van der Pijl, A. Segal, C. Vuik, P. Wesseling, A mass-conserving level-set method for modeling of multi-phase flows, *Int. J. Num. Meth. Fluids* 47 (2005) 339–361.
- [32] X.F. Yang, A.J. James, J. Lowengrub, X. M Zheng, V. Cristini, An adaptive coupled level-set/volume-of-fluid interface capturing method for unstructured triangular grids, *J. Comput. Phys.* 217 (2006) 364–394.
- [33] S.V. Patankar, *Numerical Heat Transfer and Fluid Flow*, Hemisphere, Washington, DC, 1980.
- [34] W.Q. Tao, *Numerical Heat Transfer*, second ed., Xi'an Jiaotong University Press, 2001.
- [35] C.W. Shu, S. Osher, Efficient implementation of essentially non-oscillatory shock capturing schemes, *J. Comput. Phys.* 83 (1989) 32–78.
- [36] H.A. Van Der Vorst, BI-CGSTAB: a fast and smoothly converging variant of BI-CG for the solution of nonsymmetric linear systems, *SIAM J. Sci. Stat. Comput.* 13 (2) (1992) 631–644.
- [37] H.A. Van Der Vorst, Efficient and reliable iterative methods for linear systems, *J. Comput. Appl. Math.* 149 (2002) 251–265.
- [38] J.C. Martin, W.J. Moyce, An experimental study of the collapse of fluid columns on a rigid horizontal plane, *Philos. Trans. Roy. Soc. Lond.: Ser. A* 244 (882) (1952) 312–324.
- [39] J.R. Grace, Shapes and velocities of bubbles rising in infinite liquids, *Trans. Inst. Chem. Eng.* 51 (1973) 116–120.